The equivalence between volume averaging and method of planes definitions of the pressure tensor at a plane

D. M. Heyes,[a] E. R. Smith,[b] D. Dini,[c] and T. A. Zaki[d]
Department of Mechanical Engineering, Imperial College London, Exhibition Road, South Kensington, London SW7 2AZ, United Kingdom

(Received 25 April 2011; accepted 10 June 2011; published online 13 July 2011)

It is shown analytically that the method of planes (MOP) [Todd, Evans, and Daivis, Phys. Rev. E **52**, 1627 (1995)] and volume averaging (VA) [Cormier, Rickman, and Delph, J. Appl. Phys. **89**, 99 (2001)] formulas for the local pressure tensor, $P_{\alpha,y}(y)$, where $\alpha \equiv x$, y, or z, are mathematically identical. In the case of VA, the sampling volume is taken to be an infinitely thin parallelepiped, with an infinite lateral extent. This limit is shown to yield the MOP expression. The treatment is extended to include the condition of mechanical equilibrium resulting from an imposed force field. This analytical development is followed by numerical simulations. The equivalence of these two methods is demonstrated in the context of non-equilibrium molecular dynamics (NEMD) simulations of boundary-driven shear flow. A wall of tethered atoms is constrained to impose a normal load and a velocity profile on the entrained central layer. The VA formula can be used to compute all components of $P_{\alpha\beta}(y)$, which offers an advantage in calculating, for example, $P_{xx}(y)$ for nano-scale pressure-driven flows in the x-direction, where deviations from the classical Poiseuille flow solution can occur. © *2011 American Institute of Physics*. [doi:10.1063/1.3605692]

I. INTRODUCTION

Stresses that are defined on an atomic distance scale can be used to describe the physical state of inhomogeneous systems on this scale.[1] Knowledge of the stress tensor variations in an atomistically inhomogeneous system can be used to help understand its behavior under equilibrium and non-equilibrium conditions, and suggest routes to optimise performance in use. This applies to purely solid systems (e.g., crack tip propagation in metals,[2]) and liquid-solid combinations such as high pressure elastohydrodynamic lubrication.[3] In addition, the ability to link stress profiles to atomistic interactions using non-equilibrium molecular dynamics (NEMD) simulations offers the prospect of helping to resolve some material science issues (such as the ones cited above). As a consequence, there has been significant interest in the literature in the formal definition of a local stress tensor.

In the bulk liquid state atomistic simulation literature, it is usual to focus on a second order tensor (3×3) describing the pressure, $\underline{P}$. This is equal to the negative of the stress tensor normally encountered in the continuum mechanics literature. The tensor, $\underline{P}$, is calculated using the virial formula[4]

$$\underline{P} = \frac{1}{V}\left(\sum_{i=1}^{N}\frac{1}{m_i}\underline{p}_i\underline{p}_i - \frac{1}{2}\sum_{i=1}^{N}\sum_{j\neq i}^{N}\frac{\underline{r}_{ij}\underline{r}_{ij}}{r_{ij}}\phi'_{ij}(r_{ij})\right), \quad (1)$$

where V is a volume containing N molecules, i is the index of the molecule, and m_i is its mass. If $\underline{r}_i$ is the co-ordinate of particle, i, then $\underline{r}_{ij} = \underline{r}_i - \underline{r}_j$. The translational peculiar momentum is $\underline{p}_i$,

$$\underline{p}_i = m_i(\underline{v}_i - \underline{u}(\underline{r} = \underline{r}_i)), \quad (2)$$

where $\underline{v}_i$ is the laboratory frame velocity of molecule i and $\underline{u}$ is the local advected or "streaming" velocity at spatial position $\underline{r}$. For notational simplicity, it will be assumed that the system is composed of monatomic molecules and that the pair potential, ϕ_{ij}, is therefore radially symmetric. In the above equation, the standard notation, $\phi'_{ij} \equiv d\phi_{ij}/dr_{ij}$, is used. Equation (1) is taken over a volume, V, which is assumed to be much larger than the structural correlation length in the system (typically at least 3-4 molecular diameters, σ, in a simple liquid). In bulk molecular simulation, V is the volume of the simulation cell.

The virial pressure expression given in Eq. (1) is only applicable to a homogeneous fluid, giving a single pressure tensor for the whole domain. However, a localised pressure definition is required for many NEMD applications where inhomogeneous systems are considered. One suggested local pressure tensor definition is to take each molecular term in Eq. (1) to be the pressure tensor centered on that molecule, i.e.,

$$\underline{P}_i = \frac{1}{\kappa}\left(\frac{1}{m_i}\underline{p}_i\underline{p}_i - \frac{1}{2}\sum_{j\neq i}^{N}\frac{\underline{r}_{ij}\underline{r}_{ij}}{r_{ij}}\phi'_{ij}(r_{ij})\right), \quad (3)$$

where κ is the average volume per molecule. Comparison between Eqs. (1) and (3) requires that for a bulk or homogeneous system,

$$\underline{P} = \frac{1}{V}\sum_{i=1}^{N}\kappa\underline{P}_i. \quad (4)$$

The formula in Eq. (3) could be generalised so that the local pressure tensor in a sub-volume element or "bin" of volume,

[a]Electronic mail: d.heyes@imperial.ac.uk.
[b]Electronic mail: edward.smith05@imperial.ac.uk.
[c]Electronic mail: d.dini@imperial.ac.uk.
[d]Electronic mail: t.zaki@imperial.ac.uk.

$V_{bin}(\underline{R})$, where $\underline{R}$ is a reference vector, is

$$\underline{P}_{bin}(\underline{R}) = \frac{1}{V_{bin}}\left(\sum_{i\in bin}\frac{1}{m_i}\underline{p}_i\underline{p}_i - \frac{1}{2}\sum_{i\in bin}\sum_{j\neq i}^{N}\frac{\underline{r}_{ij}\underline{r}_{ij}}{r_{ij}}\phi'_{ij}(r_{ij})\right). \quad (5)$$

The local pressure tensor in the sub-volume involves just the i particles found in that volume whereas the j particles include all possible atoms within and outside the bin. The formulas in Eqs. (3) and (5) have been shown to lead to spurious oscillations in the pressure tensor near boundaries.[5–7]

The purpose of this article is to explore and compare two now widely used statistical mechanical definitions of the local pressure tensor in the literature which can be used to resolve this quantity as a function of y, the distance perpendicular to a planar wall or boundary. This is a frequently simulated geometry in NEMD simulations, and appropriate for modelling, for example, fluid flow between solid parallel boundaries such as Couette and pressure-driven (Poiseuille) flow. These two methods are based either on a local volume average or an average of interactions across a plane. Section II considers the statistical mechanics of the local pressure tensor, and the consequences of applying external forces normal to the boundary walls. Section III reports results of NEMD simulations of boundary-driven Couette flow to compare these two methods, and conclusions are made in Sec. IV.

II. THEORY

In this section, two methods for defining the local pressure tensor are compared, and also the effects of an external force profile on this analysis are considered.

A. Planar resolution of the pressure tensor

In their pioneering paper, Irving and Kirkwood (IK) derived formulas for the pressure tensor at a point in space, $\underline{r}$, i.e., $\underline{P}(\underline{r})$.[8] Two formally equivalent expressions for $\underline{P}(\underline{r})$ were derived, one which involves an operator, O_{ij}, written as a series of particle position derivatives, and another (integral) formula where the contribution of a pair of atoms to the stress acts at points along the straight line between them. There are problems with implementing both of these representations for $\underline{P}(\underline{r})$ in any molecular simulation. If O_{ij} is set to 1, the IK formula (Eq. (2) in Ref. 6) is referred to as IK1. When V is a finite volume smaller than the simulation volume, IK1 is also incorrect for an inhomogeneous system.

A number of alternative "local" pressure tensor formulas have been derived since then. Using Fourier transformation (FT) of the momentum continuity equation, Todd *et al.* derived an expression for the local pressure tensor in terms of the force and momentum transfer across a plane, which they called the Method of Planes or "MOP."[6] An alternative formulation using an idea originally proposed by Hardy,[9] is to compute the local stress in a sub-volume of the system. Cormier *et al.*,[10] derived a formula via FT based on localising the stress in an arbitrary shaped volume, which we refer to as the volume averaging or VA method. The VA formula maintains much of the bulk virial pressure tensor form of Eq. (1), while the Todd *et al.* formula is quite different in its implementation.[6] The relationship between these two formulas for the case of the local pressure tensor for planar geometry is explored in this work. Recall that the normal or diagonal components of the pressure tensor, $P_{\alpha\alpha}$, where α is a cartesian direction, represent the force per unit area applied normal to one of the faces of a representative cubic volume orientated along the three cartesian axes, and the off-diagonal elements, $P_{\alpha\beta}$, represent a force applied parallel to the surface, per unit area.

The VA formula is[9–11]

$$\underline{P} = \frac{1}{\Omega}\left(\sum_{i=1}^{N}\frac{1}{m_i}\underline{p}_i\underline{p}_i\Lambda_i - \frac{1}{2}\sum_{i=1}^{N}\sum_{j\neq i}^{N}\frac{\underline{r}_{ij}\underline{r}_{ij}}{r_{ij}}\phi'_{ij}(r_{ij})l_{ij}\right), \quad (6)$$

where Ω is a volume of arbitrary shape and size which is less than or equal to the domain size ($\Omega \leq V$), within which the average value of $\underline{P}$ is specified. The term, Λ_i is equal to unity if particle i is in this volume and $\Lambda_i = 0$ otherwise. The quantity, l_{ij} is the fraction of $|\underline{r}_{ij}|$ which lies within the averaging volume, so $0 \leq l_{ij} \leq 1$. The volume Ω could be a sphere surrounding and containing just a single molecule. It can be seen now why the quantity $\underline{P}_i$ in Eq. (3) and the formula in Eq. (5) do *not* define the local pressure tensor of the system associated with the space immediately around the $i-$th molecule or within another specified sub-volume, as they omit the contributions of pair interactions which cross that sub-volume. In contrast, the formula in Eq. (6) permits the pressure tensor to be determined at locations in an inhomogeneous system where there are *no* molecules during the ensemble or time average process. However, the first (kinetic) part of the local pressure tensor is given correctly by the formulas in Eqs. (3) and (5).

For many atomic simulations of inhomogeneous systems, it is natural to analyse the full pressure tensor as a function of y, the cartesian component in the direction normal to a boundary wall, i.e., $\underline{P}(x, y, z)\cdot\underline{n}_y = \underline{P}(y)$, where y defines an infinite xz plane at y. For this case, the Ω volume element in the VA formula in Eq. (6) can be considered to be a "slice" or "bin" of finite thickness, Δy, in the $y-$direction which is bounded by two xz planes. Let there be N_k such bins, bounded by $y \equiv y_k \pm \Delta y/2$, where the bin location is defined to be at the mid-point y value, y_k. The optimum magnitude of Δy would be chosen to be large enough to obtain adequate statistical averaging in atomistic simulation, but small enough to resolve important fine structure in the pressure tensor profile on the atomistic scale. This means that typically $\Delta y \leq \sigma/10$, where σ is the diameter of the molecule. The local pressure tensor is decomposed into kinetic and configurational components, i.e., $\underline{P}(y) = \underline{P}^K(y) + \underline{P}^U(y)$, respectively. For the kinetic component, from Eq. (6),

$$\underline{P}^K(y_k) = \frac{1}{A\Delta y}\sum_{i=1}^{N} m_i(\underline{v}_i - \underline{u}(y_k))(\underline{v}_i - \underline{u}(y_k)) \times \theta\left(y_k + \frac{\Delta y}{2} - y_i\right)\theta\left(y_i - y_k + \frac{\Delta y}{2}\right), \quad (7)$$

where $\theta(x)$ is the Heaviside step function ($\theta(x) = 0$, $x < 0$, $\theta(x) = 1/2, x = 0$ and $\theta(x) = 1, x > 0$). A is the cross-sectional area of the simulation domain. For the configurational component, the VA formula can be written in the following analytic form,

$$\underline{P}^U(y_k) = -\frac{1}{A\Delta y}\frac{1}{2}\sum_{i=1}^{N}\sum_{j\neq i}^{N}\frac{\underline{r}_{ij}\underline{r}_{ij}}{r_{ij}}\phi'_{ij}(r_{ij})l_{ij}, \tag{8}$$

where

$$l_{ij} = \frac{|\Delta y_k|}{|y_{ij}|}, \tag{9}$$

and

$$|\Delta y_k| = \int_{y_k-\Delta y/2}^{y_k+\Delta y/2} dy\theta\Big(\frac{y_i - y}{y_{ij}}\Big)\theta\Big(\frac{y - y_j}{y_{ij}}\Big). \tag{10}$$

The quantity, $|\Delta y_k|$ is that portion of $|y_{ij}|$ which is contained within bin k. If the line, y_{ij}, passes completely through the bin, then $|\Delta y_k| = \Delta y$, whereas if i or j (only one) is in bin k, then $|\Delta y_k| \leq \Delta y$. If both i or j are in the same bin, k, then $|\Delta y_k| = |y_{ij}|$. If the line y_{ij} does not enter bin k then, $|\Delta y_k| = 0$. The ratio, $|\Delta y_k|/|y_{ij}|$ is the fraction of that ij component that contributes to $\underline{P}(y_k)$. This means that the fraction, $|\Delta y_k|/|y_{ij}|$ of the ij interaction term in the pressure tensor formula is added to the $k-$th bin entry for that quantity. It would be expected that the kinetic part of the VA pressure tensor would be more sensitive to the magnitude of Δy, than the configurational part. For $|y_{ij}| \gg \Delta y$, the configurational part should be essentially independent of Δy.

As the width of the volume element becomes smaller, Eqs. (7) and (8) approach the MOP result. For example, for $P^U_{\alpha y}(y_k)$ in this limit, i and j will have an inappreciable probability of being in the bin and Eq. (8) will reduce to

$$P^U_{\alpha y}(y_k) = \frac{1}{2A}\sum_{i=1}^{N}\sum_{j\neq i}^{N} f_{\alpha ij}\frac{y_{ij}}{|y_{ij}|}c, \tag{11}$$

where $\underline{f}_{ij} = -\underline{r}_{ij}\phi'_{ij}/r_{ij} = -\underline{f}_{ji}$ is the pair force of j acting on i, and $f_{\alpha ij}$ is the $\alpha-$cartesian component of $\underline{f}_{ij}$. The constant, c, is equal to unity when y_i and y_j are on different sides of the plane, $y = y_k$, and $c = 0$ otherwise. Equation (11) can be expressed as

$$P^U_{\alpha y}(y_k) = \frac{1}{4A}\sum_{i=1}^{N}\sum_{j\neq i}^{N} f_{\alpha ij}(sgn(y_i - y_k) + sgn(y_k - y_j)), \tag{12}$$

where $sgn(x) = 1$ for $x > 0$, $sgn(x) = 0$ for $x = 0$ and $sgn(x) = -1$ for $x < 0$. A more formal proof of this result is obtained directly from Eq. (10), which can be simplified through the substitution, $p = (y_i - y)/y_{ij}$,

$$\frac{|\Delta y_k|}{\Delta y} = \frac{1}{2\varepsilon}\int_{a-\varepsilon}^{a+\varepsilon} dp\theta(p)\theta(1-p), \tag{13}$$

where $a = (y_i - y_k)/y_{ij}$ and $\varepsilon = \Delta y/2y_{ij}$. Interest here is in the limit $\Delta y \to 0$. This is equivalent to $\varepsilon \to 0$ as Δy can always be made much smaller than $|y_{ij}|$ as $|y_{ij}| \to 0$ to achieve the $\varepsilon \to 0$ condition. Appendix A proves that the formula in Eq. (13) in the $\varepsilon \to 0$ limit is

$$\frac{|\Delta y_k|}{\Delta y} = \theta(a)\theta(1-a). \tag{14}$$

Substitution of Eq. (14) in Eq. (8) gives

$$\begin{aligned} P^U_{\alpha y}(y_k) &\to \frac{1}{2A}\sum_{i=1}^{N}\sum_{j\neq i}^{N} f_{\alpha ij}\frac{y_{ij}}{|y_{ij}|}\theta\Big(\frac{y_i - y_k}{y_{ij}}\Big)\theta\Big(\frac{y_k - y_j}{y_{ij}}\Big), \\ &= \frac{1}{2A}\sum_{i=1}^{N}\sum_{j\neq i}^{N} f_{\alpha ij}sgn(y_{ij})\theta\Big(\frac{y_i - y_k}{y_{ij}}\Big)\theta\Big(\frac{y_k - y_j}{y_{ij}}\Big). \end{aligned} \tag{15}$$

This is of the same form as found in, for example, the paper of Rao and Berne,[12] and acts as a useful intermediate step for the present treatment. Equation (15) indicates that in the limit of $\Delta y \to 0$, the number of particles in the bin tends to zero, and the interaction part of the pressure tensor on the plane is composed entirely from interactions that cross the plane. We note in passing that the above expression for the pressure tensor at a plane can also be derived directly from Irving and Kirkwood's equation (A6) found in the appendix of Ref. 8 by averaging the stress tensor at point $\underline{r}$ over an xz plane positioned at y (see Appendix B).

Equation (15) can be simplified further using $sgn(y) = 2\theta(y) - 1$ to give

$$P^U_{\alpha y}(y_k) = \frac{1}{4A}\sum_{i=1}^{N}\sum_{j\neq i}^{N} f_{\alpha ij}(sgn(y_i - y_k) + sgn(y_k - y_j)). \tag{16}$$

The formula in Eq. (16) is the interaction part of the MOP expression,[6] the local pressure tensor definition in terms of the force per unit area across a plane. The VA and MOP formulas for the local pressure tensor applied to planar geometry are therefore shown to be the same, in this special limiting case. This proof is one of the main objectives of this work. References 5, 13, and 14, for example, also consider this "mechanical" definition of local stress.

The equivalence between the planar bin VA and MOP definitions of the kinetic part of the pressure tensor, $\underline{P}^K$, in the limit of infinitely thin bin thickness can also be established.[6,15] From Eq. (7)

$$\underline{P}^K(y_k) = \frac{1}{A\Delta y}\left(\sum_{i=1}^{N}\frac{1}{m_i}\underline{p}_i\underline{p}_i\theta\left(y_k + \frac{\Delta y}{2} - y_i\right)\times\theta\left(y_i - y_k + \frac{\Delta y}{2}\right)\right). \tag{17}$$

Now consider the αy component of $\underline{P}^K(y_k)$,

$$P^K_{\alpha y}(y_k) = \frac{1}{A\Delta y}\left(\sum_{i=1}^{N}\frac{1}{m_i}p_{\alpha i}p_{yi}\theta\left(y_k + \frac{\Delta y}{2} - y_i\right)\times\theta\left(y_i - y_k + \frac{\Delta y}{2}\right)\right). \tag{18}$$

In the limit, $\Delta y \to 0$,[16]

$$P^K_{\alpha y}(y_k) = \frac{1}{A}\sum_{i=1}^{N}\frac{1}{m_i}p_{\alpha i}\,p_{y_i}\delta(y_i - y_k). \tag{19}$$

For a given time or $t-$dependent function, $g(t)$, the following delta function identity holds:

$$\delta[g(t)] = \sum_{ki}\frac{\delta[t - t_{ki}]}{|\dot{g}(t_{ki})|}, \tag{20}$$

where t_{ki} is the time when particle i crosses the plane $y = y_k$ for the ki-th time and is a root of $g(t)$. As $g(t) \equiv y_i(t) - y_k$ then $\dot{g}(t) = \dot{y}_i - \dot{y}_k \equiv p_y/m$ for the kinetic part of the pressure tensor. Let t_{sim} be the sampling or simulation time, and N_{ki} be the total number of times that particle i crosses the plane at $y = y_k$ during the simulation. On substituting Eq. (20) in Eq. (19) and using $sgn(p_{y_i}) = p_{y_i}/|p_{y_i}|$, the kinetic part of the pressure tensor in the MOP description is

$$\begin{aligned} P^K_{\alpha y}(y_k) &= \frac{1}{At_{sim}}\int_0^{t_{sim}}\sum_{i=1}^{N}p_{\alpha i}(t)\frac{p_{yi}(t)}{|p_{yi}(t)|}\sum_{ki=1}^{N_{ki}}\delta(t - t_{ki})dt \\ &= \frac{1}{At_{sim}}\sum_{i=1}^{N}\sum_{ki=1}^{N_{ki}}(\theta(t_{sim} - t_{ki}) - \theta(-t_{ki}))\,p_{\alpha i}(t_{ki}) \\ &\quad \times sgn[p_{y_i}(t_{ki})], \end{aligned} \tag{21}$$

which is the MOP definition of the kinetic part of the local pressure tensor in the case where the Heaviside functions limit the averaging period from 0 to t_{sim}. There have been many papers written using the MOP method, e.g., Refs. 17–21 and it is now an established formula, widely used in NEMD studies.

In summary, the VA formula converges in the limit of infinitely thin slice to the exact MOP formulas of Eqs. (16) and (21) for the stress across an xz plane. There are advantages in using the VA approach in certain circumstances (as will be discussed in Sec. III), as it enables all of the components of the local pressure tensor to be computed, not just $P_{\alpha y}$, which includes y as one of the cartesian indices.

The binning (VA) and the planar crossing (MOP) procedures are applicable to a range of state variables. For example, the local number density in VA form is

$$\rho(y_k) = \frac{1}{A\Delta y}\sum_{i=1}^{N}\theta\left(y_k + \frac{\Delta y}{2} - y_i\right)\theta\left(y_i - y_k + \frac{\Delta y}{2}\right), \tag{22}$$

and,[15]

$$\rho(y_k) = \frac{1}{t_{sim}A}\sum_{i=1}^{N}\sum_{ki=1}^{N_{ki}}\frac{1}{|v_{yi}(t_{ki})|}, \tag{23}$$

by the plane traversal (MOP) route,[15] where v_{yi} is the velocity of particle i in the $y-$direction.

B. The effects of an external force field

Having shown the equivalence of the VA and MOP stresses which result from interatomic forces, the following section considers the effects of external forces. In many numerical studies of inhomogeneous systems on the atomic scale, an external force field is applied to the system (e.g., in sliding friction, crack propagation and confined lubrication). While this force is not itself formally included in the definition of the pressure tensor,[8,22,23] it will indirectly influence it, as the system will need to respond to the perturbation, and possibly restructure, in order to achieve mechanical equilibrium. At steady state the following condition must be satisfied,[22]

$$\underline{\nabla}.\underline{P}(\underline{r}) + \rho(\underline{r})\underline{\nabla}\phi^e(\underline{r}) = 0, \tag{24}$$

where $\rho(\underline{r})$ is the particle number density at $\underline{r}$, ϕ^e is the external potential at point, $\underline{r}$, and $\underline{\nabla}\phi^e(\underline{r}) \equiv -\underline{F}_e(\underline{r})$ is the external force. In the present context, it is appropriate to consider a thin film geometry in which the atoms in the system are subjected to a force field which is a function of y only, then

$$\frac{\partial P_{\alpha y}}{\partial y} - \rho(y)F^e_\alpha(y) = 0, \tag{25}$$

where α can be any of the three cartesian components and $F^e_\alpha = -\partial\phi^e/\partial r_\alpha$, where r_α is the α component of $\underline{r}$. Integration of the expression in Eq. (25) between y_1 and y_2 gives

$$P_{\alpha y}(y_1) = P_{\alpha y}(y_2) + \int_{y_2}^{y_1}\rho(y)F^e_\alpha(y)dy. \tag{26}$$

For the case of a boundary constrained external force, it is convenient to choose y_1 to be in the middle of the system, i.e., $y_1 \equiv y_m$, where the magnitude of the external force is negligible, and $P_{\alpha y}(y_m)$ is determined predominantly by pair interactions between the neighboring molecules. It follows directly from Eq. (26) that the quantity on the right side of Eq. (26) is independent of y_2. Let y_b and y_t be the bottom and top limits of the particle density in the y-direction, as illustrated in Fig. 1. These are tethered solid state atoms in this study. For the bottom (b) part of the system or where $y < y_m$, the pressure tensor is denoted by $\underline{P}^b$,

$$\begin{aligned} P^b_{\alpha y}(y_m) &= P^b_{\alpha y}(y) + \int_y^{y_m}F^e_\alpha(y')\rho(y')dy' \\ &= P^b_{\alpha y}(y) + \frac{1}{A}\sum_{i=1}^{N}F^e_{\alpha,i}\theta(y_i - y)\theta(y_m - y) \equiv G(y), \end{aligned} \tag{27}$$

where $\rho(y')$ is the atomic number density at y'. The function, $G(y)$, should be independent of y, as will be shown to be the case from the simulation results presented in the figures in Sec. III. Note that, in order to achieve a physically meaningful quantity, time averaging is assumed for the last term in the above equations and corresponding terms in the equations below. For the top (t) part of the system, where $\underline{P} \equiv \underline{P}^t$ in this region,

$$\begin{aligned} P^t_{\alpha y}(y_m) &= P^t_{\alpha y}(y) + \int_y^{y_m}F^e_\alpha(y')\rho(y')dy' \\ &= P^t_{\alpha y}(y) - \int_{y_m}^{y}F^e_\alpha(y')\rho(y')dy' \\ &= P^t_{\alpha y}(y) - \frac{1}{A}\sum_{i=1}^{N}F^e_{\alpha,i}\theta(y - y_i)\theta(y - y_m) \equiv G(y). \end{aligned} \tag{28}$$

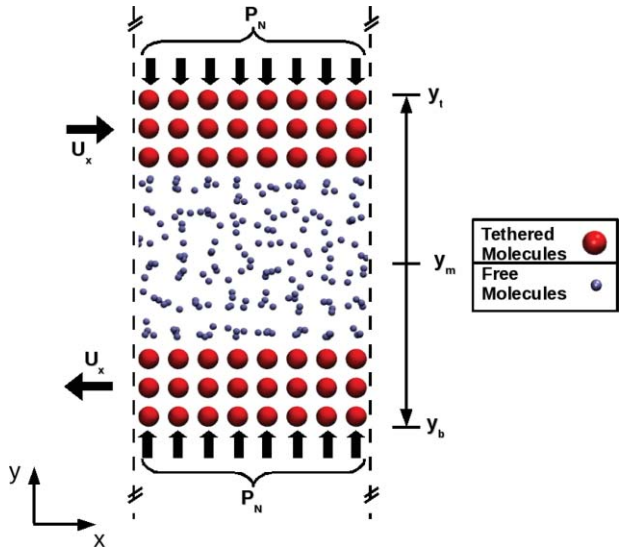

FIG. 1. Schematic diagram of the NEMD simulation geometry and key parameters. The diagram was created using VMD (Ref. 31).

The imposed pressure tensor components to the top and bottom walls are given by

$$P_\alpha^e = lim_{y\to y_b}\frac{1}{A}\sum_{i=1}^{N} F_{\alpha,i}^e\theta(y_i - y)\theta(y_m - y)$$
$$= lim_{y\to y_t} -\frac{1}{A}\sum_{i=1}^{N} F_{\alpha,i}^e\theta(y - y_i)\theta(y - y_m), \quad (29)$$

as there are no system atom-atom potential interactions crossing the $y-$plane in the limits of $y \to y_b$ and $y \to y_t$, and hence the pressure tensor terms, $P_{\alpha y}^b$ and $P_{\alpha y}^t$ tend to zero in these limits. This means that the sum of the external forces per unit area across the histogram planes at $y_k = y_b$ and $y_k = y_t$ are equal to the desired or "target" pressure tensor component, as determined from the simulation boundary conditions. Also note that from Eqs. (27) and (28),

$$P_\alpha^e = lim_{y\to y_m} P_{\alpha y}^b(y) = lim_{y\to y_m} P_{\alpha y}^t(y), \quad (30)$$

must be satisfied. The constancy of $G(y)$ throughout the system in the $y-$direction is, in fact, a restatement of Newton's principle of mechanical equilibrium (see, e.g., Ref. 24).

In the simulations whose results are discussed in Sec. III, the wall atoms are tethered to lattice sites. The tethered interactions themselves do not contribute (at least directly) to $\underline{P}(\underline{r})$ as they are one-body interactions and their contribution to the free energy, F, is therefore independent of macroscopic strain.[25] The tethering of the wall atoms does indirectly affect the pressure tensor, however, via the two-body LJ interaction contribution, as this constraint affects the particle position distribution function.

III. RESULTS AND DISCUSSION

In this section, the results of NEMD simulations are reported of boundary-driven shear flow under conditions comparable to or even more extreme than those found in typical tribological experiments.[26] The principal objective is to compare the VA and MOP formulas for the local pressure tensor, rather than being a systematic investigation of this model system through the various sets of parameters. A three-dimensional model of a nanoscale atomic sample confined in a channel between two solid walls was simulated. The channel was periodic in the streamwise, x, and spanwise, z, directions, and was bounded by solid walls on either side in the $y-$direction. The atoms in the system interacted via the Lennard-Jones (LJ) potential,

$$\phi_{kl}(r) = 4\epsilon_{kl}\left[\left(\frac{\sigma}{r}\right)^{12} - \left(\frac{\sigma}{r}\right)^{6}\right], \quad (31)$$

where the indices k and l refer to the types of atoms, either entrained phase (e) or solid wall (w). The entrained molecules can be in a liquid, glassy or polycrystalline state, depending on the imposed conditions. The cross-interaction energy parameter was the usual geometric mean of the wall-wall and entrained molecule self values, $\epsilon_{we} = (\epsilon_{ww}\epsilon_{ee})^{1/2}$. For notational simplicity below, $\epsilon \equiv \epsilon_{ee}$ is defined. The potential parameters, σ and ϵ specify the interaction range and energy, respectively. All atoms in the system had the same mass, m. A reduced temperature, $T^* = k_B T/\epsilon = 1$, where k_B is Boltzmann's constant, was employed, and $\epsilon_{ww} = 2$. The interactions were truncated at $r = 2.5\sigma$. In order to convert to real units, the LJ parameters for argon are used, where $\epsilon/k_B = 120K$, and $\sigma = 0.340$ nm. The results of the calculations are given in a mixture of LJ reduced units and real units. For pressure (stress) one LJ reduced unit is equivalent to 42.1 MPa, one LJ reduced unit of speed is equivalent to 158 m/s, and the solid wall reduced density was typically 1.063 ($\equiv$ 1.79 g/cm^3 for LJ argon).

The equations of motion and general technical procedure for carrying out the calculations were essentially those of Petravic and Harrowell (PH).[27] The wall atoms were tethered to the lattice sites with the PH anharmonic potential,

$$\Phi_T(\underline{r}_i) = k_4[\underline{r}_i - \underline{r}_{0,i}]^4 + k_6[\underline{r}_i - \underline{r}_{0,i}]^6, \quad (32)$$

where $\underline{r}_{0,i}$ is the equilibrium lattice site of atom i. The constants were, $k_4 = 5 \times 10^3$ and $k_6 = 5 \times 10^6$, in LJ units. Each confining wall was made up of 8 FCC (100) planes, allowing for a definable number of these layers to be thermostatted. The outermost layers of each wall were thermostatted to take account of the absence of an extended lattice of atoms beyond. As discussed by Bernardi *et al.*, the model for the wall can have a significant effect on the calculated properties of the liquid part of the system.[28] All wall atoms executed classical dynamics in this study (i.e., there were no "frozen" atoms).

In the MD simulation, there were three distinct regions, (r), labeled 1 for the lower solid wall and 3 for the upper solid wall. Region 2 denotes the entrained atoms between walls 1 and 3 which were free to respond to the imposed sliding and stress from the walls. An atom was associated with a particular region by virtue of its index rather than its instantaneous location. The two solid layers were constrained to move with velocities, $\underline{v}_1$ and $\underline{v}_3$, respectively, specified as input parameters. There were periodic boundary conditions in the x (flow) and z (vorticity) directions, and y is the direction perpendicular to the planes of the walls bounding the fluid. The pure sliding case, $v_3 \geq 0$ and $v_3 = -v_1$ was employed. The

system was not periodic in the y direction. For a given system size, the total force on wall atoms of regions 1 and 3 from the other atoms in the system are denoted by $\underline{F}_1^r$ and $\underline{F}_3^r$, respectively. The net force on region k from the other atoms in the system is formally defined as

$$\underline{F}_k^r = \sum_{i \in I_k} \underline{F}_i, \tag{33}$$

where $\underline{F}_i$ is the force on particle i, and I_k is the set of molecules assigned to region k. The instantaneous forces on the bottom and top walls were on average equal in magnitude and of opposite sign. The instantaneous average force on the walls was, $F_N = (F_{y3}^r - F_{y1}^r)/2$ and the instantaneous wall pressure, $P_N = |F_N|/A$, where A is the cross-sectional area of the MD cell in the xz plane.

The equations of motion for the central region molecules were integrated using the half-step leap-frog Verlet algorithm,[29] which numerically integrates Newton's equations of motion for each molecule, $\ddot{\underline{r}}_i = \underline{F}_i/m_i$, where these quantities are the acceleration, force, and mass for molecule i, respectively. The central region molecules are not thermostatted nor are they subjected to an externally imposed force or velocity field, apart from those arising through the action of the confining walls. The time step used was 0.001 in LJ reduced units.

A variety of equations of motion have been used to control the normal pressure in NEMD thin film simulations.[30] The procedure adopted here to fix the average normal pressure was to add an overdamped normal wall velocity control scheme to the PH equations of motion of the wall atoms. Let P^0 be the desired normal load pressure. Incorporating the Nosé-Hoover (NH) thermostat, the equations of motion for the wall atoms are

$$\begin{aligned} \dot{\underline{r}}_i &= \underline{p}_i/m_i + \underline{i}_x u_{k,x} \pm \underline{i}_y u_y, \\ \dot{\underline{p}}_i &= \underline{F}_i - g_m \alpha_m \underline{p}_i, \\ \dot{\alpha}_m &= (T_m - T_{m,0})/Q, \\ u_y &= (P_N - P^0)/Q_p, \end{aligned} \tag{34}$$

where $\underline{p}_i$ and $\dot{\underline{r}}_i$ are the peculiar momentum and velocity of molecule i. The time-independent normal pressure-control damping parameter, Q_p, sets the timescale of the fluctuations in the normal pressure. The choice, $Q_p = P^0$ achieved stable equilibration at the target normal pressure, P^0. The imposed drift velocity in the $x-$direction for region, k, is denoted by $u_{k,x}$, and $\underline{i}_\alpha$ is the unit vector in the $\alpha-$direction. The normal wall velocity is $\pm \underline{i}_y u_y$.

The heat generated during the simulation, which would normally have been carried away from the boundary region by an extended lattice of wall atoms, needed to be removed from the system to prevent it heating up continuously. This was performed by thermostatting the outer wall atoms. In Eq. (34), the index m is used to distinguish between the two Nosé-Hoover thermostatted regions and the remainder, which were unthermostatted. The thermostatting region parameter, g_m is equal to 1 for a thermostatted region, and $g_m = 0$ if the atom i is not in the thermostatted region. The instantaneous and desired temperatures are, T_m and $T_{m,0}$, respectively. The target temperature, $T_{m,0} = 1$ in LJ reduced units for the thermostatted region. The time-independent NH thermostatting parameter, Q, was the same for both thermostatted regions and was set to 5 in LJ reduced units. Only the outer two layers of atoms in each wall were thermostatted. Note that the velocity profile in the central region was free to adopt any form, in response to the action of the wall velocities and the values of other system parameters.

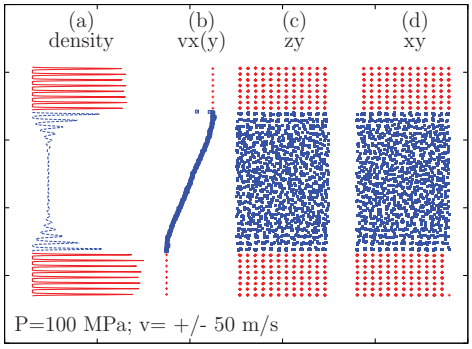

FIG. 2. (a) The normalised number density profile, $\rho(y)$, or "density" in the figure annotation. (b) the normalised $x-$velocity profile. The dots at the top and bottom are the average $x-$velocity values for each solid layer, which are seen to be the same as the imposed sliding velocity. The next two plots are snapshot projections of the assembly of particles: (c) A snapshot of the atom positions projected onto the zy plane, at the end of the simulation. z is horizontal and y is vertical. (d) A snapshot of the atom positions projected onto the xy plane, at the end of the simulation. x is horizontal and y is vertical. All atoms in the system are used in these snapshot projections. Red dots (color online) indicate wall atoms. Blue (color online) dots indicate the atoms of the entrained region. The simulation parameters are, $\epsilon_w = 2$, the Nosé-Hoover thermostat was applied to the outer two layers of each wall, the normal load was 100 MPa, the wall speeds in the $x-$direction were ± 50 m/s, and the target wall temperature, $T^* = 1$.

Figure 1 presents a schematic diagram of the simulation cell and the imposed boundary conditions. The normal pressure, $P_y^e = 100$ MPa and the wall sliding velocities of ± 50 m/s in the x direction were used.

The separation between the sampling planes for MOP and the thickness of the bin in VA were both set to $\Delta y = 0.05\sigma$. Figure 2 shows the normalised VA density profile from Eq. (22), the $x-$velocity profile and instantaneous snapshots of the particle positions projected onto two of the cartesian planes, zy and xy (the shear plane). The central region can be seen to be liquid, apart from about two layers next to the wall, where the central atoms are seen to be in registry with the walls ("epitaxial locking") as has been observed in previous such simulation studies of boundary deriven flow.[32] The velocity profile exhibits a linear velocity profile in most of the liquid region, apart from near the walls where the first few layers moved with speeds closer to those of the walls. The velocity profile becomes somewhat noisier very close to the walls as there are fewer entrained atoms on average in that region. There is no shear-induced order evident in the central region of the film. Converted to Lennard-Jones reduced units, the global shear rate for wall sliding speeds of ± 50 m/s is less than 0.03 at this pressure, which is relatively small on a molecular scale. In bulk NEMD simulations, reduced shear rates in excess of *ca.* 1 at liquid densities are typically needed to obtain shear-induced ordering at ambient pressures.[33] Heating effects can be controlled by thermostatting the wall atoms.

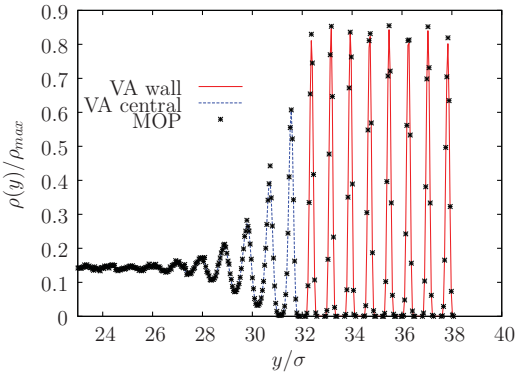

FIG. 3. The number density profiles calculated by binning or VA (continuous curves, Eq. (22)) and MOP (symbols, Eq. (23)), for the top half of the system only (i.e., $y > y_m$). Red curves indicate the wall atoms and blue curves indicate the atoms in the central liquid region. The data points are normalised by the largest density value in the entire system, ρ_{max}. The black symbols are the MOP data points while the continuous lines are for VA.

Figure 3 presents the density profile calculated by Eqs. (22) and (23) for the solid wall and central regimes. Only the top side of the system is shown, because the profile, within statistics, is symmetric, and to aid discernment of the fine structure. The figure demonstrates that there is no statistically significant difference between the density profiles computed by the two formulas, taking into account the limitations of a finite simulation length and spatial resolution of the density histogram.

The pressure tensor profiles are considered in Fig. 4 onwards, again only presenting the top half of the full profile as they are also symmetric about $y = y_m$. Figure 4 compares the $P_{yy}(y)$ profiles from the VA and MOP formulas. Again there is no statistically significant difference between the two methods. The pressure tensor decays to zero towards the outer boundaries of the walls. Also plotted on the figure is the function, $G(y)$, defined on the right hand sides of Eqs. (27) and (28). This function should be independent of y to comply with mechanical equilibrium, as it is seen to be on the figure. Note

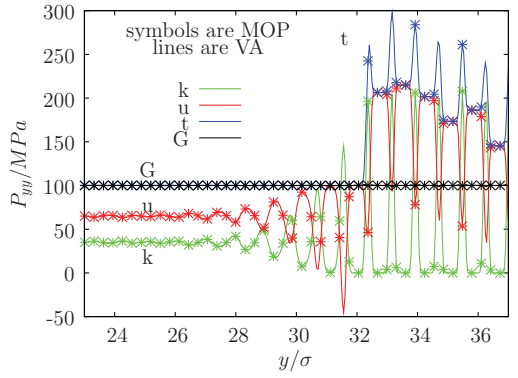

FIG. 4. The yy component of the pressure tensor, $P_{yy}(y)$, is shown. The top half of the system is shown. The individual kinetic energy and configurational components, and total value of $P_{yy}(y)$ are shown. The continuous lines are for the VA approach and the symbols are for the MOP formulas. For the VA method, the kinetic part (k) is given by Eq. (7) and the configurational part, (u) by Eq. (8). The sum of the kinetic and configurational parts is denoted by "t" on the figure. The corresponding formulas for the MOP method are Eqs. (21) and (16), respectively. "G" is the $G(y)$ function defined on the right-hand side of Eqs. (27) and (28).

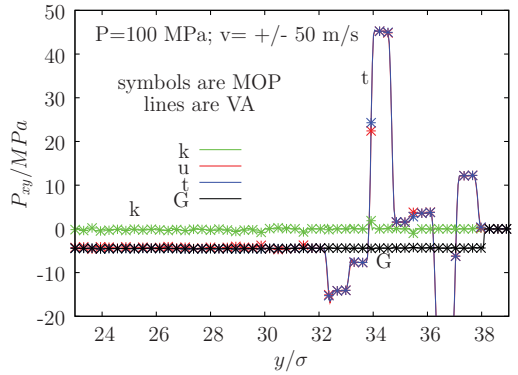

FIG. 5. As for Fig. 4 except the xy element of the pressure tensor, and its components are shown.

that, in the entrained region, oscillations in the separate kinetic and configurational parts of the pressure tensor tend to cancel each other out, to give a constant total value. Any small differences between MOP and VA can be attributed to statistical fluctuations in the simulation, of 3×10^5 time steps. Also because of the large density fluctuations in the walls, a finer spatial resolution in the pressure tensor histograms would be required for even better agreement and constancy of $G(y)$ on the figures. Other simulations carried out at an imposed normal pressure of 5000 MPa also showed that $G(y)$ is statistically constant across the system on the scale of the figure, so the methodology is robust and capable of investigating high pressure conditions typical of elastohydrodynamic lubrication and those even more extreme.

The pressure tensor element P_{xy} profile is given in Fig. 5. These data again demonstrate the good agreement between the MOP and VA expressions. $G(y)$ for this quantity is also statistically constant across the system, even in the wall regions where the density variations with distance are significant on an atomic scale. The ratio of shear to normal stress (the *traction coefficient*) is 0.04, which is a value typical for experimental lubricant systems under similar conditions.[3]

Figures 6 and 7 present the $P_{xx}(y)$ and $P_{zz}(y)$ respectively, from the VA formulas only, as there are no corresponding MOP expressions for these quantities. Also there are no external force fields in the x and z directions, and therefore no consequences from Eq. (24) for these two functions.

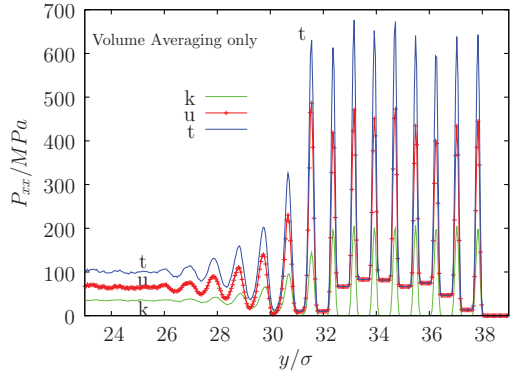

FIG. 6. As for Fig. 5 except the xx element, and its components, of the pressure tensor from the VA formulas are shown.

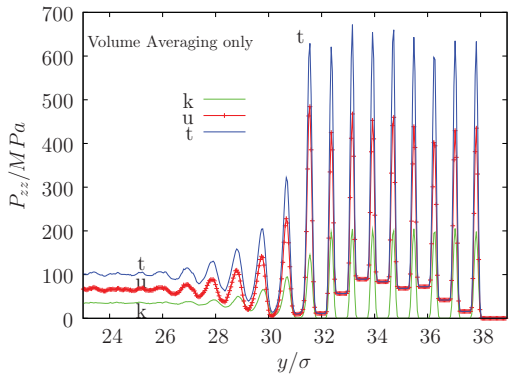

FIG. 7. As for Fig. 5 except the zz elements of the pressure tensor from the VA formulas are shown.

Nevertheless, the average pressure tensor values in the center of the film are quite close to the imposed value in the y direction (which would be expected for a hydrostatic system), i.e., $P_{xx}(y_m) \simeq P_{yy}(y_m) \simeq P_{zz}(y_m)$. In addition, note that even the *total* pressure profiles manifest significant oscillations, reflecting those in the density profile. This is perhaps not surprising as these functions are not subject to the constraints of a boundary stress (unlike P_{xy} and P_{yy}). Figures 4–7 show that the pressure tensor profiles taper off to zero towards the boundaries of the system, which reflects the diminishing number of LJ pair interactions that pass through the bin (VA) or plane (MOP) as the outer boundary of the system is approached towards the bottom and top of the system in the y direction.

IV. CONCLUSIONS

It is shown that the Method of Planes and Volume Averaging expressions for the local pressure tensor can be used interchangeably in boundary-driven flow NEMD simulations, where the cartesian coordinate (y) normal to the walls defines the spatial resolution of the pressure tensor. The VA method has the useful feature that it will give the complete pressure tensor in this geometry. It has been shown by Han and Lee,[17] that the MOP method can be extended to apply over a small finite surface rather than an infinite plane, so both VA and MOP, can be used to compute the pressure tensor variation in more complicated 2D and 3D geometries which go beyond planar localisation. If only $P_{\alpha y}$ is required, then MOP has an advantage over VA in that the potential part is exact and this result will only be approached using VA in the limit of small width of the sampling volume. If the other components of the pressure tensor are required, both methods could be used, where VA uses a coarse graining in space while Han and Lee's MOP generalisation uses coarse graining in time.

The simulations presented here have demonstrated that the VA and MOP approaches are applicable even when the external stresses are implemented indirectly, in the present case by continuously adjusting the relative velocities of the two walls to achieve an imposed normal pressure and relative sliding speed. Implementation of both methods provides a useful self-consistency check in any equilibrium molecular dynamics or NEMD application. Further investigation of the relative computational efficiencies of the two methods would be useful.

ACKNOWLEDGMENTS

The authors would like to thank Professor H. A. Spikes of the Department of Mechanical Engineering, Imperial College, London for facilitating this collaboration. The referees are thanked for helpful suggestions to improve the manuscript.

APPENDIX A: DERIVATION OF A STAGE IN THE PROOF OF THE EQUIVALENCE BETWEEN VA AND MOP FOR PLANAR GEOMETRY

The expression in Eq. (13) can be integrated by parts

$$\frac{1}{2\varepsilon}\int_{a-\varepsilon}^{a+\epsilon} dp\theta(p)\theta(1-p) = \frac{1}{2\varepsilon}[p\theta(p)\theta(1-p)]_{a-\varepsilon}^{a+\varepsilon} + \frac{1}{2\varepsilon}\int_{a-\varepsilon}^{a+\varepsilon} dp\ p\,\theta\,(p)\,\delta\,(1-p)\,, \tag{A1}$$

where the formula for the derivative of the Heaviside step function, $\frac{\partial}{\partial y}\theta\,(ay-b) = a\delta(ay-b)$, has been used. Evaluating the integral term using the sifting property of the Dirac Delta function and applying the limits of integration results in

$$\frac{|\Delta y_k|}{\Delta y} = \frac{1}{2}[\theta(a+\varepsilon)\theta(1-a-\varepsilon)+\theta(a-\varepsilon)\theta(1-a+\varepsilon)] + \frac{a}{2\varepsilon}[\theta(a+\varepsilon)\theta(1-a-\varepsilon)-\theta(a-\varepsilon)\theta(1-a+\varepsilon)] - \frac{1}{2\varepsilon}[\theta\,(1-a-\varepsilon)-\theta\,(1-a+\epsilon)], \tag{A2}$$

where ε has been canceled where it occurs on top and botttom and similar terms have been collected. Taking the limits as $\varepsilon \to 0$ using L'Hôpital's rule,

$$\lim_{\Delta y\to 0}\frac{|\Delta y_k|}{\Delta y} = \theta\,(a)\,\theta\,(1-a) - a[\delta\,(1-a)\,\theta\,(a)-\theta\,(1-a)\,\delta\,(a)] + \delta(1-a), \tag{A3}$$

the Dirac Delta functions of the form $x\delta(x) = 0$ for all x,[34] giving the final expression for the integral in the limit of the bin thickness tending to zero,

$$\lim_{\Delta y\to 0}\frac{|\Delta y_k|}{\Delta y} = \theta\,(a)\,\theta\,(1-a) + \delta\,(1-a)\,(1-a\theta\,(a))\,. \tag{A4}$$

The Dirac delta functional is only non-zero when $a = 1$. At this point, $1 - a\theta(a) = 0$ so the term is also of the form $x\delta(x)$ making it always zero. The expression for the integral over a bin in the limit of zero thickness is therefore

$$\lim_{\Delta y\to 0}\frac{|\Delta y_k|}{\Delta y} = \theta\left(\frac{y_i-y_k}{y_{ij}}\right)\theta\left(\frac{y_k-y_j}{y_{ij}}\right). \tag{A5}$$

APPENDIX B: PRESSURE TENSOR AT A POINT AND AVERAGED ACROSS A PLANE FROM THE IRVING-KIRKWOOD EQUATIONS

In this Appendix the Irving-Kirkwood (IK) formula for the pressure tensor at a point is used to define the corresponding quantity averaged over a planar surface. The IK pressure tensor at location $\underline{r}$ can be decomposed into two components, $\underline{P}(\underline{r}) = \underline{P}^K(\underline{r}) + \underline{P}^U(\underline{r})$, where $\underline{P}^K$ is the kinetic part and $\underline{P}^U$ is the configurational part,

$$\underline{P}^K(\underline{r}) = \sum_{i=1}^{N} m_i(\underline{v}_i - \underline{u}(\underline{r} = \underline{r}_i))(\underline{v}_i - \underline{u}(\underline{r} = \underline{r}_i)) \times \delta(\underline{r}_i - (\underline{r} = \underline{r}_i)), \tag{B1}$$

where $\underline{v}_i$ is the laboratory frame velocity of molecule, i, and m_i is its mass. The streaming velocity is $\underline{u}$, and $\delta(\cdots)$ is the Dirac delta function, with units of inverse volume.

Equation (A6) in Ref. 8 gives an expression for the configurational component of the pressure tensor at a point, which is written in an equivalent form as

$$\underline{P}^U(\underline{r}) = -\frac{1}{2}\sum_{i=1}^{N}\sum_{j\neq i}^{N}\frac{\underline{r}_{ij}\underline{r}_{ij}}{r_{ij}}\phi'_{ij}(r_{ij})\int_0^1 d\alpha\theta(\alpha)\theta(1-\alpha) \times \delta[\underline{r} - (\underline{r}_j + \alpha\underline{r}_{ij})], \tag{B2}$$

where $\theta(\alpha)$ is the Heaviside step function defined below Eq. (7) in the main text, and $\underline{r}_{ij} = \underline{r}_i - \underline{r}_j$. It is convenient in the present context to consider a planar spatial resolution for $\underline{r}$. The cartesian component, y replaces $\underline{r}$ on the left side of the equation in Eq. (B2)

$$\underline{P}^U(y) = -\frac{1}{2}\sum_{i=1}^{N}\sum_{j\neq i}^{N}\frac{\underline{r}_{ij}\underline{r}_{ij}}{r_{ij}}\phi'_{ij}(r_{ij})\int_0^1 d\alpha\theta(\alpha)\theta(1-\alpha) \times \delta[x - (x_j + \alpha x_{ij})]\delta[y - (y_j + \alpha y_{ij})] \times \delta[z - (z_y + \alpha z_{ij})], \tag{B3}$$

and where the Dirac delta function in $\underline{r}$ is replaced by the product of three Dirac delta functions in x, y and z, each with units of inverse length. In the above equation, the cartesian components of $\underline{r}$ are written as x, y, and z. The cartesian components of $\underline{r}_i$ are denoted by x_i, y_i, and z_i. The cartesian components of $\underline{r}_{ij}$ are written as x_{ij}, y_{ij}, and z_{ij}. Integration is carried out of x and z over the xz surface containing the x and z projections of all $\underline{r}_i$ and $\underline{r}_j$, for $0 \le x \le S_x$ and $0 \le z \le S_z$, respectively, to give the average value of $\underline{P}^U$ on this surface. A given xz surface of area $A = S_x S_z$ is located at a particular value of y. S_x and S_z could be two of the sidelengths of a parallelepiped shaped molecular dynamics simulation cell which generates a plane that is laterally homogeneous,

$$\underline{P}^U(y) = -\frac{1}{2}\sum_{i=1}^{N}\sum_{j\neq i}^{N}\frac{\underline{r}_{ij}\underline{r}_{ij}}{r_{ij}}\phi'_{ij}(r_{ij}) \times \left\{\int_0^1 d\alpha\theta(\alpha)\theta(1-\alpha)\delta[y - (y_i + \alpha y_{ij})] \times \frac{1}{S_x}\int_0^{S_x} dx\delta[x - (x_i + \alpha x_{ij})] \times \frac{1}{S_z}\int_0^{S_z} dz\delta[z - (z_i + \alpha z_{ij})]\right\}$$

$$= -\frac{1}{2A}\sum_{i=1}^{N}\sum_{j\neq i}^{N}\frac{\underline{r}_{ij}\underline{r}_{ij}}{r_{ij}}\phi'_{ij}(r_{ij})\frac{1}{|y_{ij}|}\theta\left(\frac{y_i - y}{y_{ij}}\right) \times \theta\left(\frac{y - y_j}{y_{ij}}\right). \tag{B4}$$

The above integral in α equals the value of the integrand at $\alpha = (y - y_j)/y_{ij}$, The scaling identity, $\delta(ax) = |a|^{-1}\delta(x)$,[35] has been used in the last stage in the above equation. The order of the two θ functions has been reversed to help appreciation of the meaning of their product. The integrals in x and z are unity because their limits span the simulation domain in the xz plane, and they are equal to the value of the integrand at the same value of α as the y integral. Hence, considering the components of the pressure tensor containing a y cartesian component,

$$P^U_{\alpha y}(y) \to \frac{1}{2A}\sum_{i=1}^{N}\sum_{j\neq i}^{N} f_{\alpha ij}\frac{y_{ij}}{|y_{ij}|}\theta\left(\frac{y_i - y}{y_{ij}}\right)\theta\left(\frac{y - y_j}{y_{ij}}\right), \tag{B5}$$

which is just the same as Eq. (15). Similarly for the kinetic part of the pressure tensor, we can average it over the surface. Equation (B1) gives

$$\underline{P}^K(y) = \frac{1}{A}\sum_{i=1}^{N} m_i(\underline{v}_i - \underline{u}(y = y_i))(\underline{v}_i - \underline{u}(y = y_i)) \times \delta(y - y_i). \tag{B6}$$

Equations (B4) and (B6) are quoted in the liquid-vapor interface surface tension literature.[12,36]

[1] P. Schofield and J. R.Henderson, Proc. R. Soc. London Ser. A **379**, 231 (1982).
[2] J. T. Kermode, T. Albaret, D. Sherman, N. Bernstein, P. Gumbsch, M. C. Payne, G. Csányi, and A. De Vita, Nature (London) **455**, 1224 (2008).
[3] H. A. Spikes, Lubr. Sci. **18**, 265 (2006).
[4] M. Parrinello and A. Rahman, J. Appl. Phys. **52**, 7182 (1981).
[5] K. S. Cheung and S. Yip, J. Appl. Phys. **70**, 5688 (1991)
[6] B. D. Todd, D. J. Evans, and P. J. Daivis, Phys. Rev. E **51**, 1627 (1995).
[7] F. Cleri, Phys. Rev. B **65**, 014107 (2001).
[8] J. H. Irving and J. G. Kirkwood, J. Chem. Phys. **18**, 817 (1950).
[9] R. J. Hardy, J. Chem. Phys. **76**, 622 (1982).
[10] J. Cormier, J. M. Rickman, and T. J. Delph, J. Appl. Phys. **89**, 99 (2001).
[11] J. A. Zimmerman, E. B. Webb III, J. J. Hoyt, R. E. Jones, P. A. Klein, and D. J. Bammann, Modell. Simul. Mater. Sci. Eng. **12**, S319 (2004).
[12] M. Rao and B. J. Berne, Mol. Phys. **37**, 455 (1979).
[13] D. H. Tsai, J. Chem. Phys. **70**, 1375 (1979).
[14] Z. H. Sun, X. X. Wang, A. K. Soh, and H. A. Wu, Modell. Simul. Mater. Sci. Eng. **14**, 423 (2006).
[15] P. J. Daivis, K. P. Travis, and B. D. Todd, J. Chem. Phys. **104**, 9651 (1996).
[16] C. Mack, *Fundamental Principles of Optical Lithography: The Science of Microfabrication* (Wiley, New York, 2007), Appendix C.
[17] M. Han and J. S. Lee, Phys. Rev. E **70**, 061205 (2004).
[18] J. Zhang and B. D. Todd, Phys. Rev. E **69**, 031111 (2004).
[19] H. Heinz, Mol. Sim. **33**, 747 (2007).
[20] J.-M. Simon, S. Kjelstrup, D. Bedeaux, and B. Hafskjold, J. Phys. Chem. B **108**, 7186 (2004).
[21] T. Ohara and D. Torii, J. Chem. Phys. **122**, 214717 (2005).
[22] J. S. Rowlinson, Pure Appl. Chem. **65**, 873 (1993).

[23]E. M. Gosling, I. R. McDonald, and K. Singer, Mol. Phys. **26**, 1475 (1973).
[24]S. I. Sandler and L. V. Woodcock, J. Chem. Eng. Data **55**, 4485 (2010).
[25]H. Heinz, W. Paul, and K. Binder, Phys. Rev. E **72**, 066704 (2005).
[26]G. W. Stachowiak, A. W. Batchelor, and G. Stachowiak, *Experimental Methods in Tribology*, Tribology Series Vol. 44, edited by D. Dowson (Elsevier, New York, 2004).
[27]J. Petravic and P. Harrowell, J. Chem. Phys. **124**, 014103 (2006).
[28]S. Bernardi, B. D. Todd, and D. J. Searles, J. Chem. Phys. **132**, 244706 (2010).
[29]M. P. Allen and D. J. Tildesley, *Computer Simulation of Liquids* (Oxford University Press, Oxford, 1987), p. 80.
[30]M. Lupkowski and F. van Swol, J. Chem. Phys. **93**, 737 (1990).
[31]W. Humphrey, A. Dalke, and K. Schulten, J. Mol. Graphics **14**, 33 (1996).
[32]P. A. Thompson and M. O. Robbins, Phys. Rev. A **41**, 6830 (1990).
[33]D. M. Heyes, J. Chem. Soc., Farad. Trans. II, **82**, 1365 (1986).
[34]V. K. Thankappan, *Quantum Mechanics* (Wiley, New York, 1985), Appendix D.
[35]*CRC Standard Mathematical Tables and Formulae*, 30th ed., edited by D. Zwillinger (CRC, Boca Raton, 1996), p. 72.
[36]J. P. R. B. Walton, D. J. Tildesley, J. S. Rowlinson, and J. R. Henderson, Mol. Phys. **48**, 1357 (1983).